Electronic and magnetic structure of thin Ni films on Co/Cu(001)

S. S. Dhesi, H. A. Dürr, and G. van der Laan
Magnetic Spectroscopy Group, Daresbury Laboratory, Warrington WA4 4AD, United Kingdom

E. Dudzik
Magnetic Spectroscopy Group, Daresbury Laboratory, Warrington WA4 4AD, United Kingdom
and Department of Physics, University of York, York YO1 5DD, United Kingdom

N. B. Brookes
European Synchrotron Radiation Facility, Boîte Postale 220, F-38043 Grenoble, France
(Received 25 May 1999; revised manuscript received 15 July 1999)

The electronic and magnetic structure of ferromagnetic Ni films grown epitaxially on ultrathin films of Co has been studied by x-ray-absorption spectroscopy (XAS) using circular polarization. The growth morphology of the films was verified using high-resolution low-energy electron diffraction and indicated an incomplete layer-by-layer growth mode for the Co and Ni films deposited on Cu(001). We report the presence of additional peaks in the x-ray magnetic circular dichroism (XMCD) as predicted by the configuration interaction model. The ground-state magnetic moments were obtained from the XMCD sum rules at the Ni $2p$ edge. For a film thickness below 2 ML the number of holes and the spin polarization (spin moment per hole) show a gradual decrease, while the orbital polarization (orbital moment per hole) and the spin-orbit interaction show a gradual increase in magnitude. The 6-eV satellite structure, which is present in the XAS and XMCD of bulk Ni, disappears for submonolayer coverages while the dichroism due to ''diffuse magnetism'' between the L_3 and L_2 edges is strongly enhanced. These observations are ascribed to changes in the hybridization (electronic mixing) as a function of film thickness, which influences the ground-state d^8 weight and the *s*-state spin polarization. The strongly increased orbital moment per spin provides a good measure for the degree of localization. It is shown that for Ni thin films a localization of the wave function does not lead to an enhancement in the total magnetic moment, but, on the contrary, its value is twice as small as the bulk value.
[S0163-1829(99)05241-8]

I. INTRODUCTION

Magnetic multilayers and thin films have become the subject of intense research largely stimulated by the discovery of new magnetic phenomena such as exchange biasing, giant magnetoresistance, and perpendicular magnetic anisotropy (PMA). Since the observation of PMA in Co/Pd multilayers[1] many new systems have been discovered, but the Ni/Co multilayer system is of particular interest because both constituents are ferromagnetic. In $3d$ transition-metal systems the magnetic anisotropy is intimately related to the electronic structure because the easy axis of magnetization is defined by the direction of the largest component of the orbital moment.[2–5] This sensitivity to the interface electronic structure has been demonstrated in Ni/Co multilayers where it has been shown that the PMA arises due the spin-orbit interaction of $d_{x^2-y^2}$ and d_{xy} states near the Fermi level.[6] A thorough understanding of interface electronic structure is therefore important since it strongly influences the the magnetic anisotropy through hybridization, interface roughness, and strain.

X-ray-absorption spectroscopy (XAS) using circularly polarized radiation, which gives rise to x-ray magnetic circular dichroism (XMCD), has proved to be ideal to study the electronic and magnetic properties of materials since the relevant ground-state properties can be determined using powerful sum rules.[7–9] From a detailed analysis of the Ni $L_{2,3}$ whiteline intensities of thin Ni films grown on Cu(001) Srivastava *et al.*[10] found that the density of $3d$ holes (n_h) increases by almost 20% going from a submonolayer to a 5-ML-thick film. The reduction of n_h for thin films is ascribed to a hybridization of the Cu and Ni *d* bands resulting in a charge transfer from Cu to Ni *d* orbitals.[11] Application of the sum rules to the XMCD measurements on thin Ni films on Cu(001) showed reduced spin and orbital moments compared to the bulk.[12]

The electronic structure of Ni can either be calculated with one-electron band theory[13–18] or with a configuration interaction (CI) model based on a localized Anderson impurity approach.[19–21] Korringa-Kohn-Rostoker Green's-function calculations for the ground state of Ni thin films on Cu(001) show a slight enhancement of the Ni magnetic moment at the surface but a strong reduction of the Ni magnetic moment at the Cu interface with hardly any change in the number of *d* holes.[22] The absence of a Cu magnetic moment appears to be the reason for this strong reduction in the Ni interface magnetism. For Ni on a ferromagnetic substrate, such as Co or Fe, it is therefore expected that this reduction will not occur but that Ni at the interface would retain its bulk value. However, a strong hybridization between the Ni and the substrate which changes the *d* density of states can have a significant influence on the local ground state, and hence the interface magnetism. This dilemma has motivated us to study the magnetic behavior of Ni grown on Co deposited on Cu(001).

In this paper we report on the film morphology and electronic structure of ultrathin Ni films epitaxially grown on Co films deposited on Cu(001) and we relate this information to the magnetic properties of the ultrathin Ni films. All Ni films grown on Co in this study displayed ferromagnetism which enabled the simultaneous study of magnetic and electronic properties for submonolayer coverages. XAS at the Ni $L_{2,3}$ edges was used to monitor the evolving electronic structure as a function of Ni thickness and XMCD was used to probe the element and site specific magnetic properties. The morphology and growth of the thin films were studied using high-resolution low-energy electron diffraction (HRLEED) and implied that deposition of Ni on a 4-ML Co film results in a more uniform surface with an increased average terrace width. By monitoring the modifications in the XAS and XMCD line shapes at the Ni $L_{2,3}$ edges we found that the reduced spin moment for the Ni films can be interpreted in terms of electron localization and hybridization between the Co and Ni $3d$ states.

II. EXPERIMENT

A. Growth morphology

The Cu(001) substrate was prepared by repeated cycles of Ar^+ ion bombardment and annealing to 700 K in UHV. Co was deposited onto the Cu(001) surface at temperatures between 270 and 300 K followed by deposition of Ni at similar temperatures. The films were not annealed to avoid interdiffusion and the pressure rise during deposition of either Co or Ni was $<1\times10^{-10}$ mbar. The thickness of the Ni and Co films was calibrated by a quartz crystal monitor by modulations in the specular HRLEED beam. All coverages reported in this study are accurate within 10%. The growth of Co on Cu(001) has been reported previously by several authors who have shown that for Co films $\leqslant 20$ ML a distorted fcc structure is adopted during pseudomorphic growth.[23,24] Figure 1 shows HRLEED profiles of the (00) diffraction beams from the clean Cu(001) surface, from the Cu(001) surface after the deposition of 4 ML of Co, and after the deposition of 0.3 ML of Ni on the 4-ML Co film. All HRLEED data presented here were recorded for an out-of-phase condition in order to determine changes in the average terrace size. The diffraction line shape is the sum of a sharp central peak corresponding to the long-range order and a broad structure with a width related to the average terrace width. Since the Cu(001) surface itself has an indiscernible wide feature it is clear that the Cu substrate has a high-degree of long-range order with an average terrace width exceeding the coherence length of the incident electrons ($\sim$1000 Å). Deposition of 4 ML of Co results in the appearance of a broad feature indicating a decrease in the average terrace width. Upon deposition of 0.3 ML of Ni onto the Co surface the full width at half maximum (FWHM) of this broad feature is reduced and its intensity decreases which indicates an increase in the average terrace width. From the HRLEED data it seems reasonable to suggest that at room temperature the Ni films grow by island formation at the step edges of the Co surface which results in the increased average terrace width. A more detailed study concerning the growth modes of Ni on Co/Cu(001) will be presented elsewhere.[25]

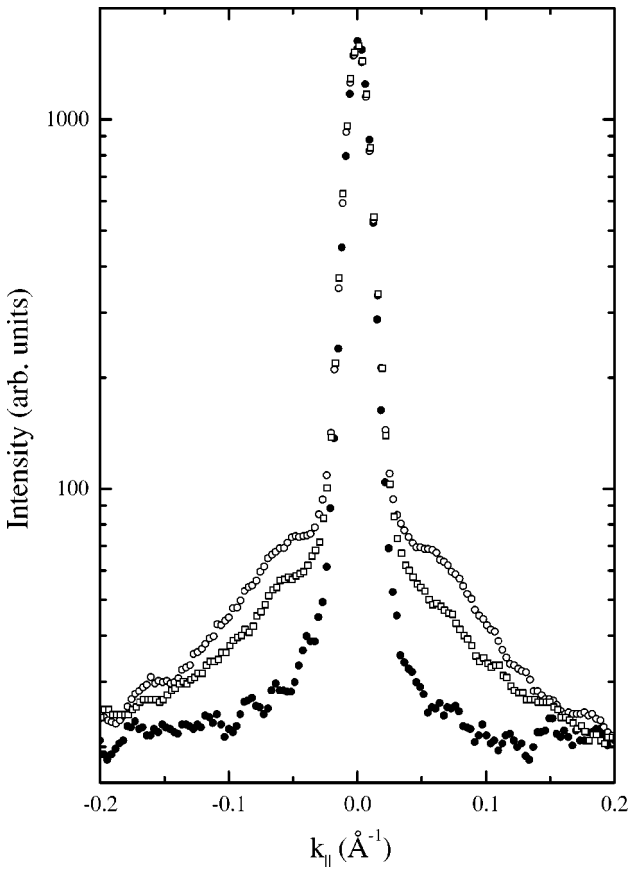

FIG. 1. HRLEED profiles of the (00) diffraction beam at the out-of phase condition from a clean Cu(001) surface (solid circles), a 4-ML Co film epitaxially grown on the Cu(001) surface (open circles), and a 0.3-ML Ni film epitaxially grown on a 4-ML Co film on the Cu(001) surface (open squares). The spectra have been normalized to the central peak and plotted on a logaritmic scale.

B. X-ray-absorption measurements

The absorption studies were performed in a separate UHV chamber, equipped with the same evaporators and sample preparation facilities as the HRLEED chamber. Measurements were done using 85% circularly polarized light from beamline ID12B of the European Synchrotron Radiation Facility (ESRF) in Grenoble. The Ni $L_{2,3}$ absorption edge was recorded in total electron yield mode with the light incident at 45° after remanent magnetization of the films perpendicular to the sample. The energy resolution of the incident x-rays was better than 0.45 eV. XMCD spectra were recorded by reversing the remanent magnetization of the thin films and by reversing the helicity of the incident radiation. All XAS spectra presented were normalized to a constant edge jump in order to obtain ground-state moments per atom. Saturation effects are negligible for the given geometry and thin Ni films used in this study. Oxidation of the film can be monitored directly from the Ni $L_{2,3}$ spectrum, since it results in a distinct change of the XAS spectrum.[26]

III. RESULTS

A. XAS

Figure 2 shows the Ni $L_{2,3}$ XAS spectra recorded with circular polarized x rays for a 2-ML Ni film epitaxially

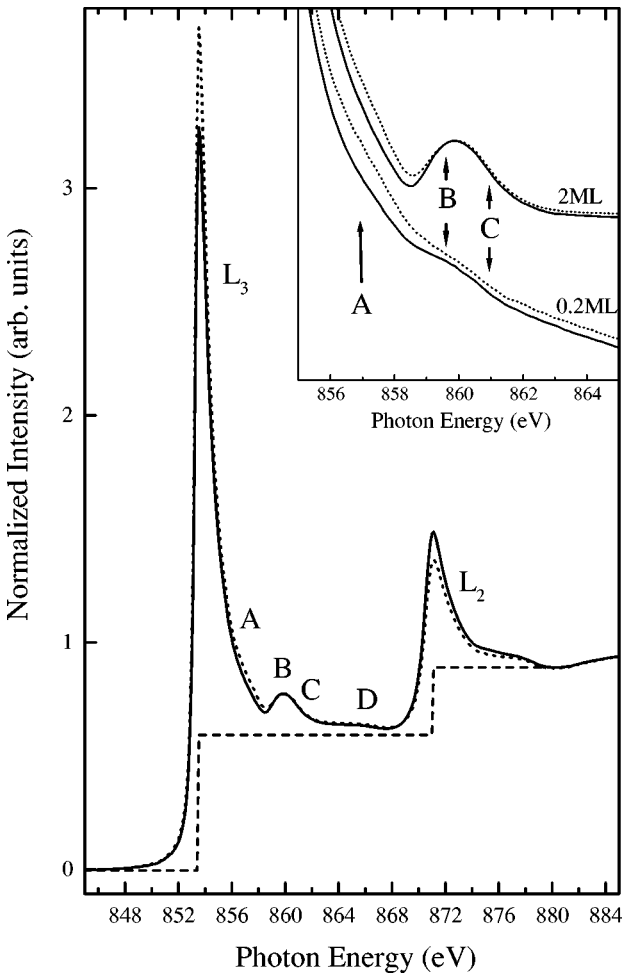

FIG. 2. Ni $L_{2,3}$ XAS measured for a 2-ML Ni film with the sample magnetization parallel (drawn line) and antiparallel (dashed line) to the photon helicity. The spectra are normalized to a constant edge jump (long dashes). The inset shows details of the 6-eV satellite above the L_3 edge for the 2-ML Ni film (top two curves) compared to a 0.2-ML Ni film (bottom two curves). The intense 6-eV satellite (marked by B) almost disappears for the thinner Ni film. Another satellite feature at 3.3 eV above the L_3 edge (marked by A) becomes visible for reduced Ni film thicknesses.

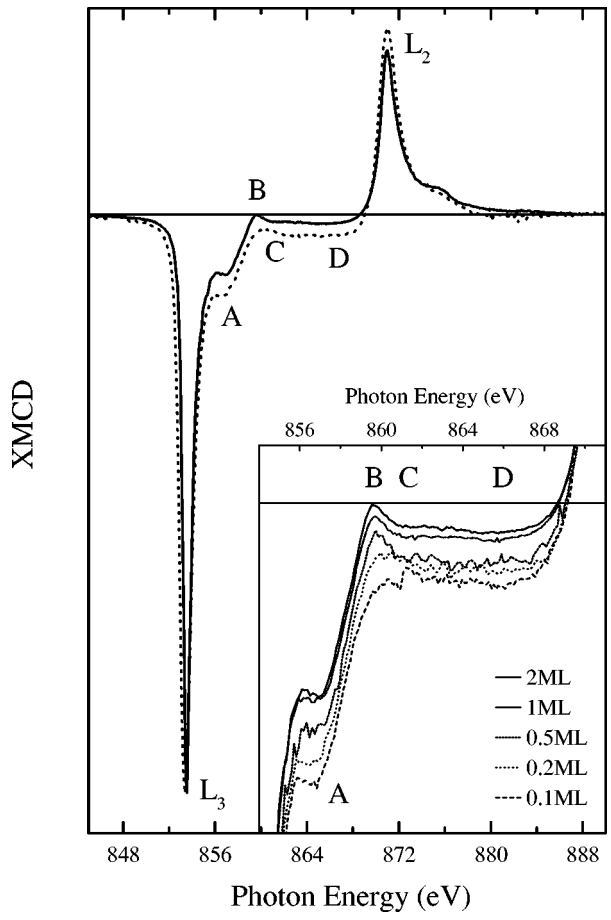

FIG. 3. Ni $L_{2,3}$ XMCD spectra for the 0.2-ML (dashed line) and 2-ML (drawn line) Ni film. The spectra were normalized to equal L_3 dichroism intensities and aligned in energy at the L_2 edge. There is a clear increase in the FWHM of the L_3 and L_2 main lines. The energy separation between the L_3 and L_2 edges increases for decreasing Ni film thickness. The inset shows the satellite structure above the L_3 edge for different Ni film thicknesses. The most remarkable change in the XMCD is the evolution of the 6-eV satellite, marked by B.

grown on a 4-ML Co film deposited on Cu(001) after remanent magnetization along the [110] and $[\overline{1}10]$ directions. The $2p$ spin-orbit interaction splits the XAS spectrum into an L_3 $(2p_{3/2})$ and L_2 $(2p_{1/2})$ structure. Different features can be distinguished above the L_3 main line, namely a high-energy tail (A), a satellite at ~ 6 eV (B) with a tail (C) and a rather structureless continuum (D). Similar features, but less distinct due to a broader linewidth, are also seen above the L_2 main line. The inset of Fig. 2 shows details in the region of the satellite structure above the L_3 edge for the 2-ML film (upper two curves) together with the XAS spectra recorded from a 0.2-ML Ni film grown on a 4-ML Co film (lower two curves). The intensity of the satellite B is strongly reduced for the 0.2-ML Ni film (downward arrow in inset of Fig. 2). There is also a weak satellite feature in the region A (upwards pointing arrow in inset of Fig. 2) which becomes more pronounced for the 0.2-ML Ni film compared to the 2-ML Ni film.

B. XMCD

Figure 3 shows the XMCD spectra for both the 0.2-ML and 2-ML Ni films obtained from the difference between XAS spectra in Fig. 2. The XMCD spectra were aligned in energy at the L_2 edge and normalized in intensity to the maximum dichroism at the L_3 edge. The spectra are dominated by the signal at the L_3 and L_2 main lines with satellite features at ~ 3.3 eV (A) and 4.0 eV above these edges, respectively. The 2-ML Ni film shows a decrease in the FWHM of the L_3 and L_2 main lines and a decrease in the energy separation between these two lines. The inset of Fig. 3 shows details of the satellite structure above the L_3 edge for different Ni film thicknesses. With increasing Ni film thickness there is a gradual reduction in the dichroic signal over the entire energy range between the L_3 and L_2 edge including the 3.3-eV satellite (A). Furthermore, the distinction of feature B is lost for the thinnest films. For comparison the XAS and XMCD of a thick Ni film are shown in Fig. 4, where peaks B, C, and D are more pronounced than in the case of the thin films.

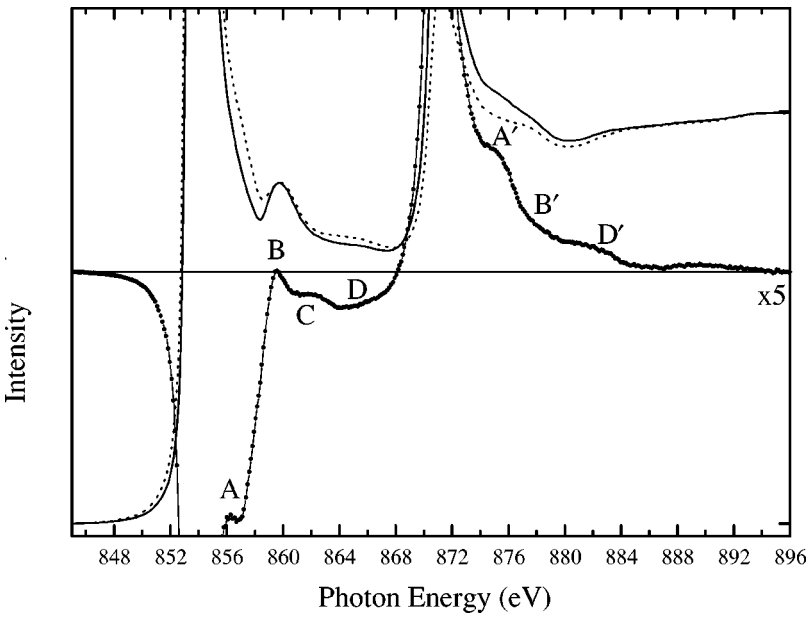

FIG. 4. Ni $L_{2,3}$ XAS measured for a thick Ni film (10 ML) with the sample magnetization parallel (drawn line) and antiparallel (dashed line) to the photon helicity; together with the XMCD (dots).

IV. DISCUSSION

Analysis of the data can be done at two separate levels of sophistication. By using the sum rules which relate the integrated signals to ground-state properties, we can draw conclusions from the experimental data which are theory independent, i.e., equally valid for a band structure and a localized description. Second, we can interpret the detailed spectral shape in terms of these different models for the electronic structure, thereby losing a certain degree of generality.

A. Sum-rules XAS

The isotropic spectrum is reasonably well approximated by the sum of the two spectra with opposite magnetization in Fig. 2. To avoid the influence of any linear dichroism due to an anisotropic $3d$ charge distribution, as reported by Srivastava *et al.*,[12] we performed our measurements near the magic angle. The integrated intensity of the isotropic spectrum, after correction for transitions into continuum states, is a measure of the number of unoccupied states in the valence band.

For the background correction of the XAS we employed the same method as, e.g., Chen *et al.*[27] for Fe and Co. To subtract the transitions into continuum states we used a step function aligned at the maxima of the L_3 and L_2 edges with relative heights of 2 : 1, which is the expected intensity ratio for transitions into the two continua. The demarcation between the integrated areas A_3 and A_2 of the L_3 and L_2 sum spectra was taken at 868.3 eV, i.e., just below the onset of the L_2 edge. The choice of this value affects the branching ratio which is a measure of the spin-orbit interaction in the valence states. It is clear from Fig. 2 that the corrected signal remains positive between the L_3 and L_2 edge and does not return to zero. A possible complication is therefore that the contribution of the L_3 structure extends further than the onset of the L_2 edge. For localized materials the L_3 structure is usually more extended than the L_2 structure,[28] which could explain why the background corrected signal in Fig. 2 does not return to zero above the L_3 edge. Therefore there is a certain degree of uncertainty in the choice of the background which will influence the absolute values of n_h and $\langle l \cdot s \rangle$ but, to a lesser extent, their trends.

Figure 5 shows the obtained branching ratio $B \equiv A_3/(A_3+A_2)$ as a function of the Ni film thickness. Whereas Ni films below 4 ML were grown on Co films, the data points at 4 ML and 10 ML are for Ni films deposited directly onto the

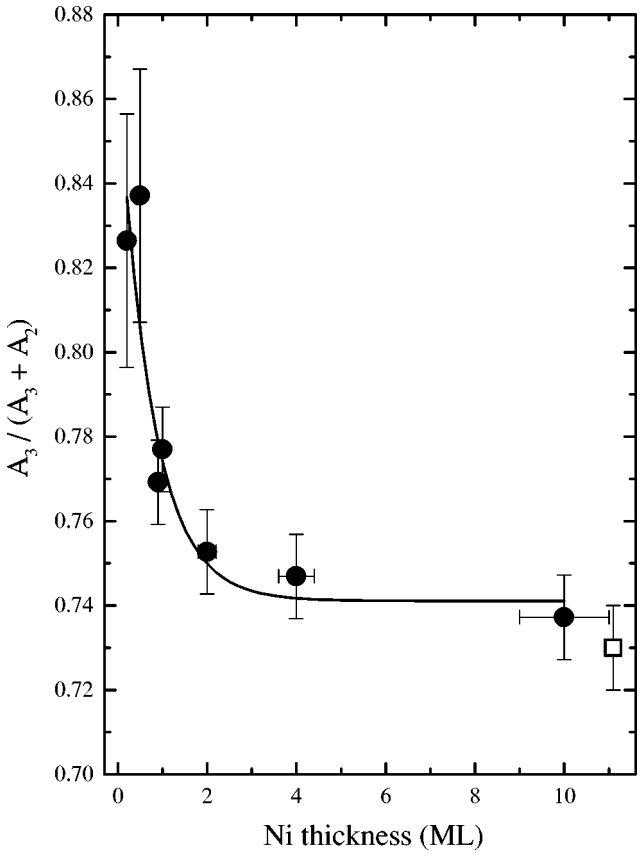

FIG. 5. Branching ratio of the background corrected integrated intensities at the $L_{2,3}$ edge as a function of Ni film thickness. The drawn line is a guide to the eye. The open square indicates the value determined for fcc Ni.[41]

Cu(001) surface. These values have been included to give supportive evidence that the electronic structure does not significantly change for a Ni film thickness above 2 ML. Taking into account that there might also be *s* states contributing to the number of holes, the branching ratio of the isotropic spectrum is given as[29]

$$B = B_0 + (B_0 - 1)\frac{\langle l \cdot s \rangle}{n_h'}, \tag{1}$$

with

$$n_h' \equiv n_h^d + n_h^s \frac{P^s}{P^d}, \tag{2}$$

where $\langle l \cdot s \rangle$ is the expectation value of the angular part of the $3d$ spin-orbit interaction, n_h^d and n_h^s are the number of *d* and *s* holes, respectively, which have transition probabilities P^d and P^s. The value of the coefficient B_0 depends on the $2p$-$3d$ electrostatic interaction, which induces *jj* mixing, i.e., a transfer of spectral weight between the two *j* edges.[29,30] For a $3d^9$ ground state there is no electrostatic interaction in the final state $2p^5 3d^{10}$ so that B_0 becomes equal to the statistical value of $\frac{2}{3}$. An admixture of $3d^8$ in the ground state will increase the branching ratio, e.g., an atomic $3d^8\ {}^3F$ state, averaged over the spin-orbit split levels, has a B_0 of ~ 0.7 (Ref. 30, Fig. 6). However, the $3d^8$ admixture in a metal is quite small, i.e., 18% in bulk Ni,[20] and even smaller for thin films as manifested by the 6-eV satellite intensity. For metallic Ni the contribution to B_0 due to core valence interaction is <0.01. If we assume that $P^d \gg P^s$ we obtain for the 10-ML film $\langle l \cdot s \rangle / n_h^d \approx 2 - 3B = -0.22$, which gradually increases to -0.48 for the thinnest films; see Tables I and II. For comparison, the Hund's rule ground state, where the spin-orbit coupling is complete, has $\langle l \cdot s \rangle / n_h^d = -1$. The measured values are quite large, and as mentioned some systematic error due to the background correction cannot completely be excluded.

B. Sum-rules XMCD

The electron expectation values of the orbital moment $\langle L_z \rangle$, spin moment $\langle S_z \rangle$, and magnetic dipole term $\langle T_z \rangle$ are related by the sum rules to the integrated XMCD signal.[7,8] Since there might also be *s* states contributing to the number of holes and to the spin moment, but not to the orbital moment and magnetic dipole term, we can write the sum rules as

$$\frac{\langle L_z \rangle}{n_h'} = \frac{4}{3}\frac{\Delta A_3 + \Delta A_2}{A_3 + A_2}, \tag{3}$$

$$\frac{\langle S_z' \rangle}{n_h'} = \frac{\Delta A_3 - 2\Delta A_2}{A_3 + A_2}, \tag{4}$$

$$\langle S_z' \rangle \equiv \langle S_z^d \rangle + \frac{7}{2}\langle T_z \rangle - 2\langle S_z^s \rangle \frac{P^s}{P^d}, \tag{5}$$

where $A_{2,3}$ and $\Delta A_{2,3}$ are the integrated sum and difference signals over the $L_{2,3}$ edges, respectively. The sum rules for $p \rightarrow d$ transitions can be retrieved by taking $P^s = 0$. Equation (5) shows that the dichroism due to the *s* spin moment is opposite in sign than that of the *d* spin moment.

The values of n_h^d and n_h^s are in principle unknown although they could be estimated from band model calculations. In order to remove the systematic error due to the background subtraction in the sum spectrum, the presence of

TABLE I. Values (with error bars) of the Ni moments per hole as obtained from the experimental spectra by applying the sum rules without making an assumption for the number of holes. $n_h' = n_h^d + n_h^s P^s/P^d$ and $\langle S_z' \rangle = \langle S_z^d \rangle + \frac{7}{2}\langle T_z \rangle - 2\langle S_z^s \rangle P^s/P^d$. The columns refer to the Ni thickness (ML), relative number of *d* holes with respect to the 10-ML film, the expectation values per *d* hole for the spin-orbit coupling, orbital moment, spin moment, and total magnetic moment, $M_z = L_z + 2S_z'$, respectively. The bottom line gives the experimental values for fcc Ni bulk.

ML	n_h'(rel.)	$\langle l \cdot s \rangle / n_h'$	$\langle L_z \rangle / n_h'$	$\langle S_z' \rangle / n_h'$	$\langle M_z \rangle / n_h'$
0.2	0.58(1)	−0.48(10)	0.07(1)	0.13(2)	0.33(4)
0.5	0.63(1)	−0.51(10)	0.06(1)	0.12(2)	0.30(4)
0.9	0.77(1)	−0.31(10)	0.05(1)	0.15(2)	0.35(4)
1	0.82(1)	−0.30(10)	0.05(1)	0.15(2)	0.35(4)
2	0.91(1)	−0.26(10)	0.05(1)	0.15(2)	0.35(4)
10	1.00(1)	−0.22(10)	0.05(1)	0.20(3)	0.45(6)
Bulk		−0.19(6)[a]	0.06(1)[b]	0.27(3)[b]	0.60(6)[b]
20[c]			0.08(1)[c]	0.29(1)[c]	0.66(2)[c]

[a]Reference 41, Ni(110) crystal.
[b]Reference 42, Ni(110) crystal.
[c]Reference 43, 20-ML Ni film on Cu(100).

TABLE II. Values (with error bars) of the total Ni moments as obtained from Table I by assuming $n_h' = 1.45$ for bulk Ni. The columns refer to the Ni thickness (ML), number of *d* holes, expectation values for the spin-orbit coupling, orbital moment, spin moment, and total magnetic moment, respectively. The bottom three lines give the theoretical values for an fcc Ni film, and the experimental and theoretical values for fcc Ni bulk. * applies only to $\langle l \cdot s \rangle$ column.

ML	n_h'	$\langle l \cdot s \rangle$	$\langle L_z \rangle$	$\langle S_z' \rangle$	$\langle M_z \rangle$
0.2	0.84(2)	−0.40(10)	0.06(2)	0.11(3)	0.28(6)
0.5	0.91(2)	−0.46(10)	0.05(2)	0.11(3)	0.27(6)
0.9	1.12(2)	−0.35(10)	0.06(2)	0.16(3)	0.38(6)
1	1.19(2)	−0.36(10)	0.06(2)	0.18(3)	0.42(6)
2	1.32(2)	−0.34(10)	0.07(2)	0.20(3)	0.47(6)
10	1.45(2)	−0.32(10)	0.07(2)	0.29(4)	0.65(8)
Film (th.)			0.09[a]	0.23[a]	0.55[a]
Bulk (exp.)	1.45*	−0.28(9)[b]	0.06(1)[c]	0.27(3)[c]	0.60(6)[c]
Bulk (th.)		−0.20[d]	0.06[e]	0.29[e]	0.64[e]

[a]Reference 17.
[b]Reference 41.
[c]Reference 42.
[d]Reference 20.
[e]Reference 40.

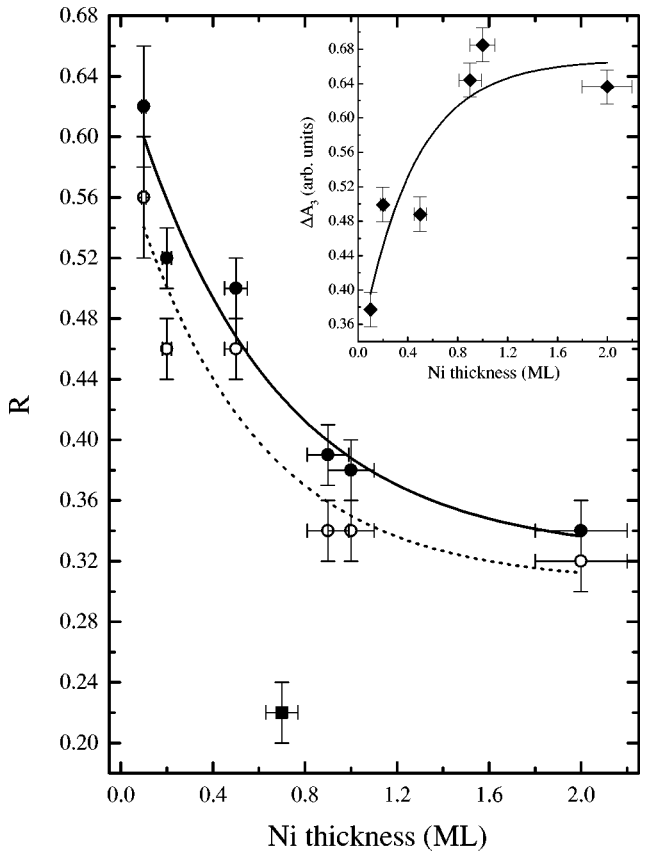

FIG. 6. Orbital moment per effective spin moment R as a function of Ni film thickness obtained from the measured XMCD using the sum rules with (closed circles) and without (open circles) inclusion of the transitions into the s and the continuum states. The lines are a guide to the eye. The closed square indicates the R value for a Ni/Co alloy. The inset shows the absolute value of the integrated area of the dichroism at the L_3 edge as a function of Ni film thickness.

linear dichroism and any incomplete polarization or magnetization, we can take the ratio

$$R \equiv \frac{\langle L_z \rangle}{\langle S_z' \rangle} = \frac{4}{3} \frac{\Delta A_3 + \Delta A_2}{\Delta A_3 - 2\Delta A_2}. \tag{6}$$

The magnetic dipole term can contribute to $\sim 10\%$ of the spin moment,[31] but we will neglect it here because our measurements were done near the magic angle.[33] In the first instance we will assume that $P^d \gg P^s$ so that $R \approx \langle L_z \rangle / \langle S_z^d \rangle$.

Table I gives the values of the Ni moments per hole as obtained from the experimental spectra by applying the sum rules without making an assumption for the number of holes. Table II gives the values of the moments per atom as obtained from Table I by assuming that bulk Ni has 1.45 holes.[10] For comparison we also give the theoretical values for an fcc Ni film, and the experimental and theoretical values for fcc Ni bulk. It should be noted that the films in this study have an fct structure, whereas the theoretical values are for the fcc phase of Ni. For a decreasing Ni thickness $\langle L_z \rangle / n_h$ increases, but there is a much stronger decrease in $\langle S_z' \rangle / n_h$, resulting in a net decrease in the total magnetic moment. Figure 6 shows the increase in R as a function of Ni film thickness obtained using sum rule analysis with (closed circles) and without (open circles) the contribution from the region above peak B in the MCXD spectra (see Fig. 3). The values of R were determined from repeated XMCD measurements with the errors representing the statistical uncertainty in the mean value of the measurements. The single data point represented by the solid square is for a Ni/Co alloy grown by codeposition of Co and Ni onto the Cu(001) surface. From the XAS edge jumps at the Ni and Co edges it is estimated that 0.7 ML of Ni was deposited with 4 ML of Co. The decrease in the value of R for the alloy is due to an increase in the spin moment, but this effect will be discussed elsewhere. Here we note only that the increased coordination of the Ni sites in the NiCo alloy leads to the dramatic reduction in the value of R which implies that the thin Ni films grown on the Co film in this study do not form an alloy. The inset of Fig. 6 shows the integrated L_3 signal of the XMCD spectra as a function of Ni film thickness. The sharp decrease in magnitude of the dichroism for a Ni film thickness below 1 ML indicates that the magnetic moment is quenched for the lower coverages. Table II shows that for the thinnest Ni film $M_z = L_z + 2S_z$ is two times smaller than for the bulk. On the other hand, for the thinnest film R is 2.4× larger than for the bulk.

The increase in R for the thin coverages is due the reduced spin moment and also arises from a small increase in the orbital moment because of the reduced crystal field of the surface atoms. The latter lifts the quenching of the spin-orbit coupling and hence the orbital moment. An increase in the spin-orbit coupling per hole leads to an increase in the orbital moment per spin. Table I shows an almost linear relation between the two quantities $\langle l \cdot s \rangle / n_h$ and $\langle L_z \rangle / \langle S_z' \rangle$. However, a strictly linear proportionality is merely fortuitous, since such a relation would also depend on the details of the electronic structure near the Fermi level.

C. Spectral structure

For bulk nickel Chen *et al.*[32] already reported the satellite at ~ 3.3 eV above the L_3 edge in the XMCD. However, the ~ 6 eV satellite, which is visible in the XAS, was reported to be absent in the XMCD. In Chen's paper the satellites in the XMCD and XAS are marked with B and A, respectively, but here we will mark them as A and B, respectively. Our high-resolution measurement reveals much more structure which make it more practical to label these features with increasing photon energy (cf. the bulk spectrum shown in Fig. 4). Theoretical calculations based on the CI model[20] have also predicted the presence of additional structure in the XMCD, such as the positive feature around 6 eV. The reason for the satellite structure is that the $2p^5 3d^9$ final state configuration is split by core-valence exchange interaction into a singlet and triplet spin state. The triplet state, where the spins of the core and valence holes are parallel, has the lowest energy and corresponds to satellite A. The singlet state at higher energy corresponds to the satellite B. Without spin-orbit coupling the singlet state cannot be reached from a triplet $3d^8$ initial state, but the large $2p$ spin-orbit interaction allows spin-flip transitions which brings the singlet final state into reach.

In order to understand the satellite structure, it is instructive to consider first the x-ray absorption from a pure $3d^8$

initial state into a $2p^5 3d^9$ final state, as occurs in divalent Ni compounds. The experimental XMCD spectrum for Ni^{2+} in $NiFe_2O_4$ provides a good starting point for our discussion and can be found in Fig. 1 of Ref. 34, where the features denoted by A, B, C, and D correspond to the satellites marked with the same labels in Figs. 2, 3, and 4 of this paper. The L_3 edge of Ni^{2+} is mainly split into a doublet A-B which is a measure for the effective $2p$-$3d$ exchange interaction screened by intra-atomic relaxation. The energy splitting of ~ 2.6 eV, observed for Ni metal, suggests a $2p$-$3d$ exchange interaction which can be expected for a localized model. Atomic calculations show that the dichroic signal of satellite B is always smaller than that of satellite A. The intensity ratio depends on both the $2p$-$3d$ exchange interaction and the crystal-field interaction. For a moderate or strong crystalline field the dichroism of the features A and B have opposite sign.[34] Since the exchange interaction can be determined from the A-B separation, the intensity ratio can be used as a measure for the crystal-field interaction in the d^8 ground state.[34] The corresponding L_2 edge is also split into a doublet structure, but the core hole $j=1/2$ character together with the $2p$-$3d$ exchange interaction result in a reduced energy separation and in a different intensity ratio. The XMCD at the L_2 edge is entirely positive, lacking features with opposite sign such as in the L_3 edge.

Returning to the case of nickel, for the metal we have to take into account the hybridization of the $2p^5 3d^9$ configuration with other configurations, of which the $2p^5 3d^{10}$ will be the most important. The character of each final state will be a mixture of the pure configurations. Due to the Coulomb interaction the $2p^5 3d^{10}$ configuration has the lowest energy and has therefore the highest weight in the main peak. The main peak is most strongly mixed with the triplet final state (A) which has the smallest energy separation. Each state is broadened by band effects, which leads to an overlap in energy, so that the triplet state will become part of the high-energy tail of the main peak. The evolution of the XAS satellite structure (Fig. 2) shows that this effect depends on the coverage. Peak A is located within the main band, so that its intensity smears out. However, for submonolayer coverage where the hybridization is smaller, peak A becomes more distinct.

In the XAS, satellite B practically disappears for the 0.2-ML coverage. This can be explained by a reduced Ni-Co hybridization (proportional to the square root of the number of neighbors) with decreasing coverage, which diminishes the $3d^8$ weight in the ground state. Then the $2p^5 3d^9$ final state can no longer be reached.

In the XMCD (Fig. 3) the positive signal of peak B on a negative background is clearly visible. This feature has escaped earlier XMCD studies on Ni which have all been taken at a lower photon energy resolution. This feature loses its distinction for submonolayer coverage where the hybridization is reduced.

The feature C, a small increase in the negative dichroism (Fig. 3), might be due to excited crystal-field states. The negative dichroism in the region D between the L_3 and L_2 edges is ascribed to transitions into empty s states which are strongly spin polarized (cf. Sec. IV D) together with possibly higher excited final states, such as $2p^5 3d^8$ which may give rise to the increase in the negative dichroism in region D of Fig. 4.

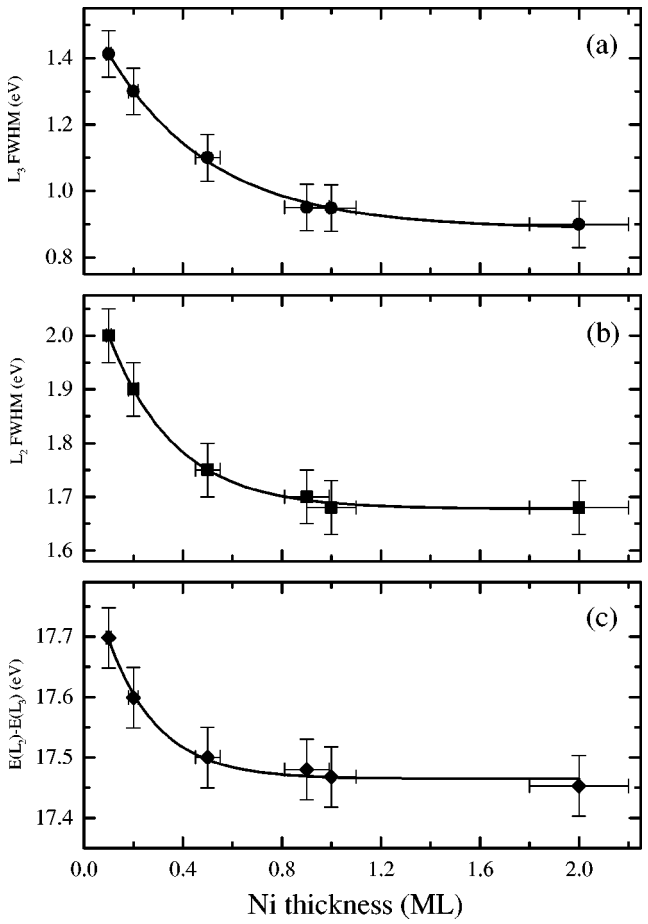

FIG. 7. (a) Ni L_3 and (b) Ni L_2 main peak FWHM in the XMCD, and (c) energy separation between the L_3 and L_2 XMCD main lines as a function of Ni film thickness. The drawn lines are a guide to the eye.

Figure 7 shows that the energy separation between the L_3 and L_2 main lines increases for the submonolayer coverage by several tenths of eV. Systematic calculations[35] show that the energy splitting due to the $2p$ spin-orbit interaction is independent of the d count, so that this effect can be excluded. Since the relative intensities and separations of the satellites are different for the L_3 and L_2 edge, a change in coverage which induces different d weights might give a very small change in the energy separation of the $L_{2,3}$ main lines. Figure 7 shows the FWHM of the dichroism at the L_2 and L_3 edges as a function of Ni coverage. The increase in the FWHM at the L_3 and L_2 edges is most likely due to an energy shifted component which decreases in intensity with increasing Ni film thickness. The energy shifted component is also seen in the XAS spectra from thin Ni films, but disappears for a Ni film thickness above 1 ML. In addition, it is this shifted component which results in the shift in energy of the L_3 edge relative to the L_2 edge. Since the shifted component essentially disappears during the submonolayer regime it must be related to modifications in the surface electronic structure. In the submonolayer regime island formation at step edges is the most likely growth mode for the Ni films so that the shifted component may be related to

the electronic structure of individual Ni islands. The coordination of the Ni atoms within an island differs between the center and the perimeter so that as the film thickness is decreased the perimeter atoms contribute more significantly to the XAS spectra line shape. Previous studies of Co nanoclusters[36] indicate that as the diameter of a cluster is reduced the perimeter atoms become more important in terms of the electronic structure and result in an energy shifted component in XAS spectra.

D. Diffuse magnetism

The core-valence Coulomb interaction pulls down final states with localized $3d$ character compared to those with s character, so that the latter will be at higher photon energy. Therefore the nonzero dichroism observed between the L_2 and L_3 edge is expected to be at least in part due to the spin polarization of empty s states. Alternatively, the dichroism could be due to configurations such as $2p^5d^8$. However, since the dichroism is decreasing as a function of coverage while the satellite structure should decrease, we might only for the thickest coverages expect a contribution from the $2p^5d^8$ configuration. The remaining dichroism is therefore ascribed to ''diffuse magnetism.''[37] In accordance with the common usage, the spin contributions to the magnetic moment can be separated into local and diffuse parts, where local part means the $3d$ contribution and diffuse part means the sp contribution, which is also that part of the moment whose density lies mainly in the interstitial region of the crystal and is not detected in neutron-diffraction experiments under normal circumstances.[38] In Fe, Co, and Ni the relative signs of the diffuse and local moments are opposite due to hybridization between the $3d$ and sp electrons, which exceeds the exchange interaction.[39]

For fcc bulk Ni the calculated diffuse magnetism is -7% of the spin moment,[40] while neutron scattering give gives -17%. In XMCD it represents an integrated intensity of about 5%. This would suggest that the cross sections for excitation into the s states are quite similar to those into the d states, while calculations indicate that they should be at least an order of magnitude larger. Also the diffuse magnetism is apparently absent above the L_2 edge where it should appear with equal intensity but positive sign, since the integrated intensity over both edges should vanish because the s states have no orbital moment. One possible explanation is that the s and d states are strongly mixed, which becomes possible in lower than cubic symmetry, such as for the thin film.

V. CONCLUSIONS

X-ray-absorption measurements of well characterized Ni thin films on Co/Cu(001) as a function of coverage have provided several interesting results. Using the sum rules for a straightforward determination of the ground-state magnetic moments, we find that with decreasing film thickness the number of d holes and the spin polarization (spin moment per hole) are decreasing, while the orbital polarization (orbital moment per hole) and the spin-orbit interaction are increasing. Furthermore, there are striking changes in the spectral structure for submonolayer coverages. The 6-eV satellite structure (peak B) disappears in both XAS and XMCD, and the dichroism due to ''diffuse magnetism'' between the L_3 and L_2 edge is strongly enhanced at low coverages. In a configuration interaction model, peak B can be ascribed to a $2p^53d^9$ final state with singlet character. The diffuse magnetism is due to empty s states with opposite spin polarization than the empty d states.

These observations indicate that the electronic mixing (hybridization) changes as a function of film thickness. The hybridization is proportional to the square root of the number of neighbor atoms. When it reduces, such as at the surface, the d^8 weight in the ground state reduces, which is evidenced by the disappearance of satellite B. The triplet final state (peak A) is not reduced because it has considerable mixing with the nearby state that forms the main peak. The localization of the wave function increases the intra-atomic mixing between the d and s states, which is manifested by the increase in s-spin polarization.

Localization of the d states and reduced crystal-field interaction at the surface enhances the atomiclike properties such as the orbital polarization and the spin-orbit interaction. However, the spin polarization decreases because the driving mechanism, the high-spin d^8 in the ground state, disappears. The orbital moment per spin is therefore strongly increased and provides a good measure for the localization of the d wave function. It is interesting to note that localization in the case of Ni thin films does not result in an enhanced total magnetic moment, on the contrary the magnetic moment is two times smaller than in the bulk.

This research was supported under EPSRC Grant No. GR/L38240. We thank K. Larsson for his help and technical assistance.

[1] P. F. Carcia, A. D. Meinhaldt, and A. Suna, Appl. Phys. Lett. **47**, 178 (1985).
[2] P. Bruno, Phys. Rev. B **39**, 865 (1989).
[3] D. Weller, J. Stöhr, R. Nakajima, A. Carl, M. G. Samant, C. Chappert, R. Mégy, P. Beauvillain, P. Veillet, and G. A. Held, Phys. Rev. Lett. **75**, 3752 (1995).
[4] H. A. Dürr, G. Y. Guo, G. van der Laan, J. Lee, G. Lauhoff, and J. A. C. Bland, Science **277**, 213 (1997).
[5] G. van der Laan, J. Phys.: Condens. Matter **10**, 3239 (1998).
[6] See, e.g., *Ultrathin Magnetic Structures* edited by B. Heinrich and J. A. C. Bland (Springer, Berlin, 1994).
[7] B. T. Thole, P. Carra, F. Sette, and G. van der Laan, Phys. Rev. Lett. **68**, 1943 (1992).
[8] P. Carra, B. T. Thole, M. Altarelli, and X. Wang, Phys. Rev. Lett. **69**, 2307 (1993).
[9] G. van der Laan, Phys. Rev. Lett. **82**, 640 (1999).
[10] P. Srivastava, N. Haack, H. Wende, R. Chauvistré, and K. Baberschke, Phys. Rev. B **56**, R4398 (1997).
[11] D. Wang, A. J. Freeman, and H. Krakauer, Phys. Rev. B **26**, 1340 (1982).
[12] P. Srivastava, F. Wilhelm, A. Ney, M. Farlew, H. Wende, N.

Haack, G. Ceballos, and K. Baberschke, Phys. Rev. B **58**, 5701 (1998).
[13] J. L. Erskine and E. A. Stern, Phys. Rev. B **12**, 5016 (1975).
[14] R. Wu, D. Wang, and A. J. Freeman, J. Magn. Magn. Mater. **132**, 103 (1994).
[15] R. Wu and A. J. Freeman, Phys. Rev. Lett. **73**, 1994 (1994).
[16] H. Ebert, Rep. Prog. Phys. **59**, 1665 (1996).
[17] O. Hjortstam, J. Trygg, J. M. Wills, B. Johansson, and O. Eriksson, Phys. Rev. B **53**, 9204 (1996).
[18] G. Y. Guo, Phys. Rev. B **55**, 11 619 (1997).
[19] T. Jo and G. A. Sawatzky, Phys. Rev. B **43**, 8771 (1991).
[20] G. van der Laan and B. T. Thole, J. Phys.: Condens. Matter **4**, 4181 (1992).
[21] G. van der Laan, Int. J. Mod. Phys. B **8**, 641 (1994).
[22] A. Ernst, S. S. Dhesi, W. M. Temmerman, and G. van der Laan (unpublished).
[23] H. Li and B. P. Tonner, Surf. Sci. **237**, 141 (1990).
[24] O. Heckman, H. Magnan, P. le Fevre, D. Chandesris, and J. J. Rehr, Surf. Sci. **312**, 62 (1994).
[25] S. S. Dhesi, H. A. Dürr, and G. van der Laan (unpublished).
[26] F. May, M. Tischer, D. Arvanitis, M. Russo, J. Hunter Dunn, H. Henneken, H. Wende, R. Chauvistré, N. Mårtensson, and K. Baberschke, Phys. Rev. B **53**, 1076 (1996).
[27] C. T. Chen, Y. U. Idzerda, H.-J. Lin, N. V. Smith, G. Meigs, E. Chaban, G. H. Ho, E. Pellegrin, and F. Sette, Phys. Rev. Lett. **75**, 152 (1995).
[28] G. van der Laan and B. T. Thole, Phys. Rev. B **43**, 13 401 (1991).
[29] G. van der Laan and B. T. Thole, Phys. Rev. Lett. **60**, 1977 (1988).
[30] B. T. Thole and G. van der Laan, Phys. Rev. B **38**, 3158 (1988).
[31] J. Stöhr and H. König, Phys. Rev. Lett. **75**, 3748 (1995).
[32] C. T. Chen, F. Sette, Y. Ma, and S. Modesti, Phys. Rev. B **42**, 7262 (1990).
[33] G. van der Laan, Phys. Rev. B **57**, 5250 (1998).
[34] G. van der Laan, C. M. B. Henderson, R. A. D. Pattrick, S. S. Dhesi, P. F. Schofield, E. Dudzik, and D. J. Vaughan, Phys. Rev. B **59**, 4314 (1999).
[35] G. van der Laan and I. W. Kirkman, J. Phys.: Condens. Matter **4**, 4189 (1992), Table 3.
[36] H. A. Dürr, S. S. Dhesi, E. Dudzik, D. Knabben, G. van der Laan, J. B. Goedkoop, and F. U. Hillebrecht, Phys. Rev. B **59**, R701 (1999).
[37] W. L. O'Brien, B. P. Tonner, G. R. Harp, and S. S. P. Parkin, J. Appl. Phys. **76**, 6462 (1994).
[38] M. B. Stearns, in *Numerical Data and Functional Relationships in Science and Technology*, edited by H. P. J. Wijn, Landolt-Börnstein, New Series, Group 3, Vol. 19, Pt. A (Springer, Berlin, 1986).
[39] O. K. Andersen, J. Madsen, U. K. Poulsen, O. Jepsen, and J. Kollar, Physica B & C **86-88B**, 249 (1977).
[40] O. Eriksson, A. M. Boring, R. C. Albers, G. W. Fernando, and B. R. Cooper, Phys. Rev. B **45**, 2868 (1992).
[41] J. Vogel and M. Sacchi, Phys. Rev. B **49**, 3230 (1994).
[42] J. Vogel, G. Panaccione, and M. Sacchi, Phys. Rev. B **50**, 7157 (1994).
[43] W. L. O'Brien and B. P. Tonner, Phys. Rev. B **50**, 12 672 (1994).